Ligand-Free and -Bound Structures of the Binding Protein (LivJ) of the *Escherichia coli* ABC Leucine/Isoleucine/Valine Transport System: Trajectory and Dynamics of the Interdomain Rotation and Ligand Specificity†

Sergei Trakhanov,[‡,§] Nand K. Vyas,[‡] Hartmut Luecke,[∥] David M. Kristensen,[⊥] Jianpeng Ma,[‡,⊥,#] and Florante A. Quiocho*[,‡,⊥]

Verna and Marrs McLean Department of Biochemistry and Molecular Biology and Graduate Program of Structural and Computational Biology and Molecular Biophysics, Baylor College of Medicine, Houston, Texas 77030, Department of Molecular Biology and Biochemistry, University of California, Irvine, California 92697, and Department of Bioengineering, Rice University, Houston, Texas 77005

Received December 22, 2004; Revised Manuscript Received February 15, 2005

ABSTRACT: The leucine/isoleucine/valine-binding protein (LIVBP or LivJ) serves as the primary high-affinity receptor of the *Escherichia coli* ABC-type transporter for the three aliphatic amino acids. The first structure of LIVBP determined previously without bound ligand showed a molecule comprised of two domains which are far apart and bisected by a wide open, solvent-accessible cleft. Here we report the crystal structures of another ligand-free state and three complexes with the aliphatic amino acids. In the present ligand-free structure, the two domains are farther apart. In the three very similar complex structures, the two domains are in close proximity, and each desolvated ligand is completely engulfed in the cleft and bound by both domains. The two different ligand-free structures, combined with those of the very similar ligand-bound structures, indicate the trajectory and backbone torsion angle changes of the hinges that accompany domain closure and play crucial functional roles. The amino acids are bound by polar and nonpolar interactions, occurring predominantly in one domain. Consistent with the protein specificity, the aliphatic side chains of the ligands lie in a hydrophobic pocket fully formed following domain or cleft closure. Comparison of the structures of LIVBP with several different binding proteins indicates no correlations between the magnitudes of the hinge-bending angles and the protein masses, the ligand sizes, or the number of segments connecting the two domains. Results of normal-mode analysis and molecular dynamics simulations are consistent with the trajectory and intrinsic flexibility of the interdomain hinges and the dominance of one domain in ligand binding in the open state.

Bacteria rely heavily on the binding protein-dependent ABC-type active transport systems for uptake of nutrients even in severe conditions of limiting or very low concentrations. In *Escherichia coli* alone, there are approximately 50 of these systems for uptake of diverse sets of nutrients, including carbohydrates (monosaccharides and oligosaccharides), amino acids, dipeptides and oligopeptides, polyamines, vitamins, cations, tetrahedral oxyanions, organophosphonate and organosulfonate, choline/taurine, heme, etc. (*1*, *2*). The binding proteins serve as the initial high-affinity ligand receptor and conduit for delivering the ligand or substrate to the protein membrane components for translocation across the cytoplasmic membrane. At least six binding proteins further act as receptors for chemotaxis (*2*). The binding proteins, with mass ranging from 25 to 60 kDa and little amino acid sequence similarity, reside freely in the periplasmic space of Gram-negative bacteria or are anchored via a thiol−lipoyl group on the cell surface of the outer cell wall of Gram-positive bacteria. They have specificities that vary from the more loose to the most stringent. Examples of those with looser specificity include the maltose-binding protein (MalE), which recognizes linear oligosaccharides with two to seven glucose units and cyclic maltodextrins (*3*), and the dipeptide-binding protein (DppA) or oligopeptide-binding protein (OppA), which binds dipeptides or oligopeptides, respectively, with the nature of the side chains being unimportant (*4*). The specificities of the binding proteins (PstS, Sbp, and ModA) for the tetrahedral oxyanions (phosphate, sulfate, and molybdate, respectively) are some of the most stringent, a remarkable feat for structurally very

† The work was supported by grants from the Welch Foundation to J.M. and F.A.Q., the NIH (R05 GM56445-06 to H.L. and R05 GM02138-27 to F.A.Q.), and the Howard Hughes Medical Institute to F.A.Q. J.M. is a recipient of the Award for Distinguished Young Scholars Abroad from the National Natural Science Foundation of China. This paper is dedicated to the memory of Alexei Nickitenko.

* To whom correspondence should be addressed. Phone: 713-798-6565. Fax: 713-798-8516. E-mail: faq@bcm.tmc.edu.

‡ Verna and Marrs McLean Department of Biochemistry and Molecular Biology, Baylor College of Medicine.

§ Present address: Sinsheimer Laboratories, RNA Center, University of California at Santa Cruz, 1156 High St., Santa Cruz, CA 95064.

∥ Department of Molecular Biology and Biochemistry, University of California at Irvine.

⊥ Graduate Program of Structural and Computational Biology and Molecular Biophysics, Baylor College of Medicine.

Department of Bioengineering, Rice University.

10.1021/bi047302o CCC: $30.25
Published on Web 04/05/2005

similar substrates. These stringent specificities guarantee that the translocation of a nutrient as crucial as the phosphate is not inhibited by the other oxyanions. The diversity of ligands has made the superfamily of ABC-transport binding proteins a gold mine for detailed investigations particularly of protein−ligand recognition. These investigations, especially employing X-ray crystallography, have uncovered basic features of recognition (*5*). The focus of this paper is on the Leu/Ile/Val-binding protein (LIVBP)[1] of *E. coli*.

Leu/Ile/Val-binding protein (or its present designation of LivJ) (*6*) is, as its original and more descriptive name implies, able to bind all three branched chain aliphatic amino acids. Other requirements for the substrates include free α-amino and α-carboxy groups and L-stereochemistry. Interestingly, there is also a leucine-specific binding protein (or LivK) in *E. coli* (*6*), which is very similar in sequence and crystal structure to LIVBP (*7*). These strong similarities are consistent with the fact that active transports via LivJ and LivK use the same cytoplasmic membrane-bound protein and ATPase components (*6*).

The crystal structure of LIVBP in the ligand-free form was the third to be determined from the binding protein superfamily (*8*), being preceded by the substrate-bound structures of D-arabinose-binding protein (or AraF) (*9*, *10*) and D-galactose/D-glucose-binding protein (or MglB) (*11*, *12*). Even with only three different crystal structures solved, several features of the ABC-type transporter binding proteins emerged (*8*), which would prove eventually to be shared by all subsequent structures of at least two dozen different binding proteins (unpublished data; see also ref *5*). The salient features are as follows. (1) Despite the lack of a uniform size and high sequence similarity, the structures of the binding proteins are very similar overall, comprising two globular domains with β/α fold separated by a cleft or groove. (2) The substrate binds within the cleft/groove and is completely enclosed by the two domains. (3) In sharp contrast to the ligand-bound structures, the ligand-free structure has the two domains farther apart and the cleft wide open and accessible to the bulk solvent. This observation of a dramatic difference between the ligand-bound or "closed" cleft structure and ligand-free or "open" cleft structure provided the clearest evidence for a bending motion of a hinge between the two domains [aptly called "Venus' flytrap" model (*13*)] that plays important roles in ligand binding and signal transduction in active transport and chemotaxis.

Here we report the crystal structures of a ligand-free LIVBP that has a more open cleft than that observed previously and of the three complexes with leucine, isoleucine, and valine. The three similar structures of the closed state, combined with those of the two different open states, indicate the trajectory and the molecular nature of the interdomain rotation, the atomic features that restrict binding of only amino acids and only those with aliphatic side chains, and the interplay between nonpolar and polar interactions in ligand recognition. Finally, normal-mode analysis and targeted molecular dynamics simulations were carried out to further understand the large interdomain motion and ligand binding along the pathway of the conformational changes.

[1] Abbreviation: LIVBP, leucine/isoleucine/valine-binding protein.

EXPERIMENTAL PROCEDURES

Protein Purification and Removal of Bound Endogenous Ligand to Purified LIVBP. The procedure for the purification of native LIVBP from *E. coli* has been described previously (*14*). Like most binding proteins, native purified LivJ contains a bound ligand.

To remove completely and easily any bound endogenous amino acids to LIVBP, the purified protein was subjected to two gel filtration chromatographies onto Sephadex G-50 columns; the first column was equilibrated with 7 M urea in 10 mM sodium/potassium phosphate (pH 7.3) buffer, and the second column was equilibrated with only the buffer. The protein was added onto the first column and eluted with the same buffered urea solution. The protein was then added onto the second column and eluted with only the buffer in order to allow initial refolding of the protein on the column. The protein was then incubated in the cold room to ensure complete renaturation, which was monitored by UV spectral change that is observed upon addition of L-leucine (*15*). The ligand-free LIVBP, concentrated to 10−15 mg/mL 10 mM sodium/potassium phosphate (pH 7.3), was used in all of the crystallization described below of the ligand-free and ligand-bound states. This ensures that the structure of each complex with a ligand is not contaminated by an endogenous bound amino acid.

Crystallization and Structure Determination of LIVBP in the "Superopen" State. For crystallization, the ligand-free protein was mixed with an equal volume of the precipitant [12.5% PEG-6000, 25 mM KCl, 25 mM NaCl, 0.01% NaN_3, 10 mM potassium acetate, 5 mM sodium citrate (pH 4.5)]. Aliquots of 50 μL of the protein solution were placed into microdialysis cells and dialyzed against 5 mL of the precipitant solution in the cold room. Crystals usually appeared after several days. Diffraction data were collected to 1.7 Å resolution on an SDMS two-detector system mounted on a Rigaku RU200 X-ray generator (Cu Kα radiation) equipped with a graphite crystal monochromator operated at 110 mA and 40 kV and processed by a program associated with the detector.

The structure of the ligand-free LIVBP was solved successfully by molecular replacement using the original 2.4 Å LIVBP ligand-free structure (*8*) as the search model in MERLOT (*16*). The rotation function (module CROSUM) yielded a maximum for Euler angles $\alpha = 90°$, $\beta = 81°$, $\gamma = 280°$ against all F_o greater than 5σ in the resolution shell 8−4 Å. The peak height is 5.4 times above standard deviations and 30% higher than the next highest peak. The rotation solution was subsequently refined with a three-dimensional search using the LATSUM module with 1 deg increment to 88°, 83°, 280°. The solution of the translation function was equally straightforward. The molecular translations were $t_x = 0.3019$, $t_y = 0.2967$, $t_z = 0.2153$ in fractional coordinates. Following application of the rotation and translation values to the search model, the entire molecule was subjected initially to rigid-body refinement in X-PLOR. Subsequently, the entire molecule was divided into four individual segments (residues 11−121, 122−248, 249−329, and 330−344) and allowed to move independently. The initial *R*-crys dropped from 0.492 to 0.326 for the 8−4 Å resolution shell. This was followed by several rounds of positional simulated annealing and *B*-factor refinement in

Table 1: Data Collection and Refinement Statistics for Leucine/Isoleucine/Valine Binding (LIVBP) with and without Bound Ligand

item	bound ligand			
	none (superopen)	Leu	Ile	Val
		Intensity Data Collection		
divalent metal additive	none	1 mM Cd^{2+}	10 mM Cu^{2+}	50 mM Cd^{2+}
space group	$P2_12_12_1$	$P6_4$	$P3_121$	$P2_12_12_1$
a (Å)	57.21	87.65	99.13	58.42
b (Å)	65.29	87.65	99.13	70.34
c (Å)	109.61	94.04	93.18	82.90
angle (deg)	$\alpha = \beta = \gamma = 90$	$\alpha = \beta = 90, \gamma = 120$	$\alpha = \beta = 90, \gamma = 120$	$\alpha = \beta = \gamma = 90$
Z	1	1	1	1
D_{min}[a] (Å)	1.70	1.72	1.96	2.10
no. of observations	168430	108495	153626	66070
no. of unique reflections	42957	37508	31814	18896
completeness (%)/last shell	96/89	86/60	83/40	92/85
R_{merge}[b] (%)/last shell	6.9/27.7	5.9/25.0	5.1/18.4	12.9/24.2
$\langle I/\sigma(I)\rangle$/last shell	9.8/1.9	11.7/1.8	15.3/2.5	5.4/2.2
last shell (Å)	1.75−1.7	1.86−1.72	2.10−1.96	2.20−2.10
		Refinement		
R-crys/*R*-free[c]	18.7/22.5	17.5/21.1	18.2/20.5	21.6/26.3
no. of atoms				
protein	2591	2591	2591	2591
ligand	none	9	9	8
solvent	228	232	351	195
metal cation	none	1 Cd^{2+}	none	3 Cd^{2+}
others	none	none	MPD	none
rmsd				
bond lengths (Å)	0.011	0.010	0.011	0.011
bond angles (deg)	1.7	1.5	1.6	1.6
dihedral angles (deg)	24.0	23.2	23.1	23.5
improper angles (deg)	1.1	1.0	1.1	1.0

[a] D_{min} = the smallest *D* spacing for which reflections were measured. [b] $R_{merge} = \sum_i(\sum_j|I_{ij} - \langle I_i\rangle|)/\sum_i\langle I_i\rangle$; I_{ij} is the scaled intensity of the *j*th observation of each unique reflection *i*; $\langle I_i\rangle$ is the mean value. [c] *R*-factor $= \sum_{hkl}||F_o| - |F_c||/\sum_{hkl}|F_o|$, where $|F_o|$ and $|F_c|$ are the observed and calculated structure factor amplitudes for reflection *hkl*, applied to the work (*R*-crys) and test (*R*-free) (5−10% omitted from refinement) sets, respectively.

X-PLOR/CNS (*17*, *18*). After each round, the fit of the model to the density was investigated and, if necessary, corrected manually on a computer graphics system using CHAIN (*19*). The current *R*-crys is 18.7% and *R*-free is 22.5% for the 1.7 Å resolution data (Table 1).

Structure Determination of the LIVBP−Leucine Complex. The procedure for the crystallization of the native protein with bound L-leucine follows that described previously (*14*). Thick hexagonal prism crystals ($0.3 \times 0.3 \times 1.0$ mm^3) of the complex were routinely grown in the cold room using the hanging drop method in the presence of 1 mM Cd^{2+}. The cation additive was crucial in obtaining the large crystals. The crystals belong to the $P6_4$ space group (Table 1).

Intensity data from one LIVBP crystal were collected as described above to 1.72 Å resolution, and the statistics are shown in Table 1. The structure was determined by molecular replacement using as the search model the 1.7 Å structure of LIVBP solved in the ligand-free state (described above; see also Table 1) that had been transformed to the closed state using the graphics program CHAIN (*19*). This approach has been previously used successfully in our laboratory in the structure determination of the histidine-binding protein using the open state of the lysine/arginine/ornithine-binding structure as the search model (*20*). Modeling the LIVBP closed state was guided by the relative orientation between the two domains observed for the closed state structures of several binding proteins (*5*). The Cα backbone of the LIVBP open state was displayed on a graphics system, and the two domains were manually rotated about a hinge in the segments connecting the two domains in order to bring the two domains close to each other without steric interference between residues in both domains. The complete structure for each domain was then superimposed on the Cα backbone trace.

Using the modeled LIVBP closed state led to a straightforward molecular replacement solution in X-PLOR (*17*). After filtration the highest peak in the rotational search exceeds the next peak by 1.25-fold. Following rotation of the model by $\theta_1 = 289°$, $\theta_2 = 68°$, and $\theta_3 = 245°$, a translation search yielded a strong peak (20σ peak height). The model was translated $t_x = 0.133$, $t_y = 0.267$, $t_z = 0$ and subjected to rigid body refinement with the two domains allowed to move independently. This lowered the *R*-crys to 38% in the resolution range 8−3 Å. The *R*-crys dropped further to 27% after the first round of positional refinement in the resolution range 8−2.5 Å. The structure was finally refined as described above for the ligand-free protein to 1.72 Å (Table 1).

Crystallization and Structure Determination of the LIVBP−Isoleucine Complex. Crystallization of the LIVBP in the presence of isoleucine was carried out by the hanging drop method in the cold room. To exploit the positive effect of divalent cations on crystallization, 10 mM $CuSO_4$ was added to the crystallization mixture. Bulky hexagonal crystals grew in 1 week in drops made by mixing 1 part of the 10 mg/mL stock protein and 1 part of the precipitant solution of 30% 2-methyl-2,4-pentanediol, 10 mM $CuSO_4$, 0.5 mM L-isoleucine, and 50 mM sodium cacodylate (pH 5.0) and placed over 1 mL of the precipitant solution. The crystals belong to the $P3_121$ space group (Table 1). A single crystal was

mounted in a hair loop and, flash cooled by immersing into a liquid nitrogen bath, and data were collected as described above. Statistics of the data collection are shown in Table 1.

The refined structure of the LIVBP−Leu complex (with the coordinates for the Leu deleted) determined as described above was used as the search model in a clear-cut molecular replacement solution of the structure of the LIVBP−Ile complex. The highest peak in the rotational search remained on the top of the list of peaks after filtration and exceeded the next peak by about 25%. Following rotation of the model by $\theta_1 = 249.1°$, $\theta_2 = 177.6°$, $\theta_3 = 208.7°$, a translation search yielded a strong peak (19σ peak height) which was 37% higher than the next solution. Following translation of the model ($t_x = 0.133$, $t_y = 0.267$, $t_z = 0$), rigid body refinement with the two domains allowed to move independently reduced the *R*-crys to 0.311. The structure was finally refined in CNS to 1.96 Å resolution as described above (Table 1).

Structure Determination of the LIVBP−Valine Complex. In addition to the prime objective of obtaining high-resolution diffracting crystals of the LIVBP−valine complex, we wanted to explore the possibility that dicarboxylic acids (e.g., succinate) and Cd^{2+} could act in facilitating protein crystallization by bridging neighboring protein molecules, the succcinates between basic residues and Cd^{2+} between acidic groups. The crystal screen was prepared as a multidimensional matrix, varying the cadmium salt concentration in one dimension and the dicarboxylic acid concentration in another dimension. Also, the concentrations of PEG-400 precipitant and the pH values of the solutions were varied.

Crystals of prismatic morphology with dimensions $0.2 \times 0.3 \times 0.7$ mm^3 were obtained at cold room temperature in the presence of 1 mM valine by the hanging drop method. The precipitant was composed of 25% (v/v) PEG-400, 0.1 M succinic acid, 50 mM $CdSO_4$, and 50 mM sodium cacodylate (pH 5.5). The drop was formed by mixing 5 μL of protein solution ($\sim$10 mg/mL) and 5 μL of the precipitant solution and hung on a siliconized cover slip.

Data from a single crystal after "flash cooling" into a liquid nitrogen bath were collected as described above to 2.1 Å resolution (Table 1). The search for a molecular replacement solution used the structure of the LIVBP−Leu complex (with the coordinates of Leu removed) and EPMR program of Kissinger and Gehlhaar (ftp.augoron.com). The very first solution resulted in a correlation coefficient of 0.684 and *R*-crys of 0.381 for all data in the resolution shell 15−4 Å. The model was rotated by $\theta_1 = 23.38°$, $\theta_2 = 81.59°$, and $\theta_3 = 270.75°$ and translated by $t_x = 56.68$ Å, $t_y = 24.93$ Å, and $t_z = 29.43$ Å. This model was subjected to several rounds of refinement in X-PLOR and ARP (*21*). The statistics of the refinement at 2.1 Å are shown in Table 1.

Deposition of Coordinates and Structure Factors. Coordinates for the four crystal structures described above have been deposited in the Protein Data Bank (accession codes: 1Z15, LIVBP superopen form; 1Z16, 1Z17, and 1Z18, LIVBP with bound leucine, isoleucine, and valine, respectively).

Normal-Mode and Molecular Dynamics Analyses. The normal-mode analysis was performed on the open state. The structure was energy minimized by 1000 steps of the steepest descent method followed by a few thousand steps of the Adapted Basis Newton Raphsen method (*22*); the minimizations were terminated when the rms energy gradient had been reduced to 10^{-27} kcal mol^{-1} Å^{-1}. Then the low-frequency modes were computed by the CHARMM package (*22*). The CHARMM parameter 19 was used for potential function (*23*).

The trajectory between the Ile-bound and ligand-free open states of the LIVBP protein was calculated using targeted molecular dynamics (TMD) (*24*). This method was implemented with the CHARMM program (*22*) using standard potentials with an additional time-dependent constraining force that slowly pulls the molecule toward the final state, in this case the open, unbound state. This dynamic constraint was applied only to the protein, not to water molecules. Before equilibration, the closed state of the protein (with isoleucine bound) was superimposed onto a previously equilibrated system consisting entirely of water molecules using the TIP3 model (*25*) in order to provide a shell of explicit water molecules extending to 5 Å from the protein. Water molecules within 2.8 Å of a protein atom were excluded from this superimposition, leaving 1041 explicit water molecules. The resulting system was equilibrated in several stages, whereby each stage first performed 1000 steps of energy minimization, followed by a 100 ps dynamic equilibration. At first, only the water was allowed to move while the protein was restrained. Next, the side chains were allowed to move, although a constant harmonic force restrained the atoms. In the final step, the entire protein was allowed to move and equilibrate with only a small constant harmonic force restraining the atoms in the system. After 500 ps of equilibration, an additional 500 steps of minimization and 50 ps of equilibration were performed before the actual TMD simulation of 500 ps with a time step of 1 fs. The temperature of the system was kept near 300 K by coupling the system to a heat bath with a relaxation time of 0.1 ps. In addition, the length of all bonds involving hydrogen atoms was constrained by the SHAKE algorithm (*26*). The standard leapfrog algorithm was used for integrating the equations of motion. The TMD simulation was performed four times, each with a different random seed value but otherwise with identical input parameters.

Illustrations. Figures 1, 2, 3A, 4, and 5B were prepared by using MOLSCRIPT (*27*). Figure 5A was prepared by using VMD (*28*).

RESULTS

Structure Determination. All four structures reported here were determined by the molecular replacement technique and refined against diffraction intensity data (2.1−1.7 Å resolution) collected from in-house equipment to *R*-crys values that range from about 18% to 22% and *R*-free values from 21% to 26% and to good geometry (Table 1).

Crystallization Additives. Although it was relatively easy to crystallize the ligand-free state of LIVBP during the time when crystallization kits were not even available (*8*), it was only recently that we have been able to crystallize the ligand-bound state of LIVBP (*14*). There was no one condition that enabled the crystallization of the one unbound and three bound forms. However, cation additives were crucial in obtaining high-resolution diffracting crystals of the bound form. This was demonstrated initially for the complex with

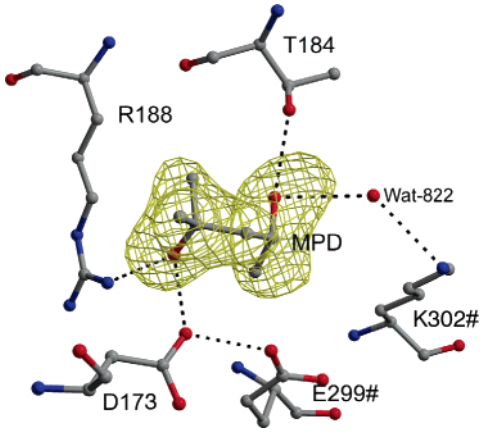

FIGURE 1: 2-Methyl-2,4-pentanediol bound between LIVBP molecules in the structure of the complex with Ile (Table 1). The difference Fourier map is contoured at 3σ. Residues marked with the symbol # are from a symmetry-related protein molecule.

Leu, which yielded thick hexagonal prism crystals (*14*) (see also Experimental Procedures). In the absence of cations, crystals grew as long thin needles (*14*). Cd^{2+} (1 mM) was used in obtaining the crystal of the LIVBP−Leu complex whose structure is reported here. Surprisingly, however, only one Cd^{2+} metal (Table 1) was clearly evident in the refined structure, which was located between two different molecules (data not shown). Crystallization of the complex with valine required a higher concentration Cd^{2+} (50 mM). Although succinate was also included in the solution used to crystallize the protein in the presence of Val, none was visible in the structure. Moreover, of the three Cd^{2+} metals identified in the Val-bound structure (Table 1), only one was found bound between different molecules. The Cd^{2+} metals in the complexes with Leu and Val were chelated mostly by carboxylate side chains.

Although $CuSO_4$ was required for obtaining crystals of the LIVBP−Ile complex (Table 1), no Cu^{2+} or SO_4^{2-} could be found in the crystal structure. However, one molecule of the precipitant 2-methyl-2,4-pentanediol (MPD) was observed mediating indirect interactions between two symmetry-related protein molecules (Figure 1). Two hydroxyl groups of the MPD are involved in the interactions. One of the interactions is linked through a water molecule. Thus, it is possible for MPD to mediate intermolecular contacts which may facilitate crystal formation.

Ala 47 to Val Change in the Sequence and a Rare Cis Peptide Bond Conformation. With only one exception, the original amino acid sequence of LIVBP, which was determined by chemical and DNA sequencing methods (*29*, *30*), is confirmed by the four refined structures. The exception is Ala 47 in both sequence determinations, which is clearly a valine as indicated in the electron density (see Figure 2A). The residue in the equivalent location in the leucine-specific binding protein is also valine (*7*). Since the valine residues in both proteins are far (~20 Å) from the ligand-binding site, it has no relevance to complex formation.

The four structures (Table 1) also revealed a cis conformation of the Gly 75−His 76 peptide bond (Figure 2B). The occurrence in protein structures of a cis ω dihedral angle for a peptide bond X−Y, where Y is not a Pro residue, is very rare, amounting to only about 0.05% (*31*, *32*). The cis conformation is not the product of crystal packing since all four structures (liganded and unliganded) are in totally different lattice arrangements (Table 1). There is nothing to suggest that the His residue is in an unusual or special location as it is neither in contact with other molecules in the four different space groups nor in proximity to the bound ligands and the three segments connecting the two domains. We attribute the cis bond formation to the constraint imposed by the formation of a string of hydrogen bonds tying up the His side chain and the backbone carbonyl oxygen. As depicted in Figure 2B, the two nitrogens of the imidazole ring make hydrogen bonds with the side chains of Asp 51 and Tyr 89, the former as an acceptor and the latter as a donor, and the main chain peptide bond carbonyl oxygen is coupled, through a water molecule, to Asp 51. It is noteworthy that the equivalent residue (His 76) in the leucine-specific binding protein also adopts a cis conformation (S. Trakhanov and F. A. Quiocho, unpublished data).

Overall Three-Dimensional Structure. As revealed by the first structure of LIVBP determined at 2.4 Å resolution (*8*), the protein is divided into two globular domains [named I and II or N- and C-domains, respectively, in previous designations (*8*)] with similar β/α fold (Figure 3A). With three segments linking both domains, each domain is folded from two separate segments from both the amino- (or N-) and carboxy- (or C-) terminal halves of the polypeptide chain. Although the three interdomain segments are widely separated in the sequence, they are in close proximity to each

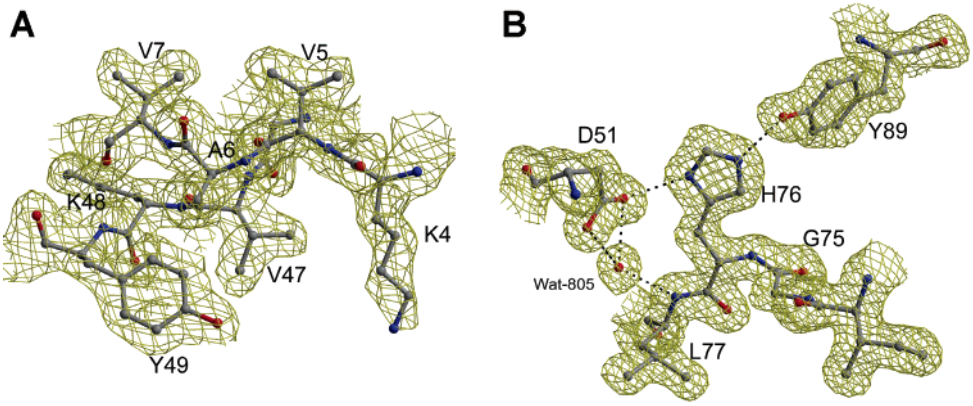

FIGURE 2: Two notable residues (Val 47 and His 76) in the four structures (Table 1) of LIVBP. The electron density maps are $2F_o - F_c$ contoured at 1σ. Data are from the LIVBP−Leu complex structure. (A) Replacement of Ala 47 in the original primary sequence by a Val residue. (B) Cis conformation of the Gly 75−His 76 peptide bond.

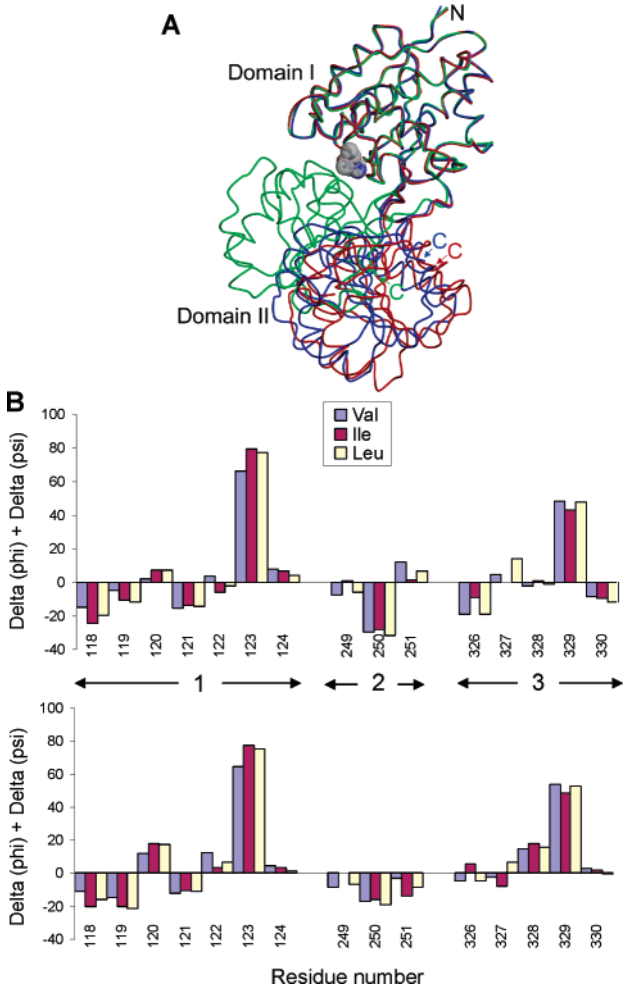

FIGURE 3: Interdomain rotation or domain closure. (A) Three different crystal structures of LIVBP. Domain I (or N-domain as identified in previous papers) (*7*, *8*) of the closed, Ile-bound (green), open (blue), and superopen (red) structures is superimposed. The atoms of the Ile bound in the cleft between the two domains in the closed form structure are represented in semitransparent van der Waals spheres. The N and C labels mark the amino and carboxy termini. As discussed in the main text, the ligand binds preferentially to domain I in the open state, which could be represented by one of the open states (colored red or blue) with the Ile bound as shown in the closed state (colored green). (B) Plots of the sum of $\Delta\phi + \Delta\psi$ for the domain closure from the open (top) and superopen (bottom) states to the closed state with bound Val (blue), Ile (red), and Leu (yellow). Data are taken from Table 4. Residue segments corresponding to hinges 1, 2, and 3 are delimited by arrows.

other in the tertiary structure (Figure 3B) and, as a consequence, form the base of the ligand-binding site cleft between the two domains and further act as a set of hinges for interdomain rotation which plays crucial functional roles (discussed further below). Interdomain segments 1 and 3 extend from domain I to domain II, whereas segment 2 runs in the opposite direction. Segments 1 and 2 are preceded by a β-sheet strand in one domain and followed by an α-helix in the other domain, whereas segment 3 bridges strands from both domains.

Open and Closed States of LIVBP. The three structures of LIVBP with bound Leu, Ile, and Val, identified as "closed state", are very similar as indicated by rmsd values of ~0.25 Å between the overlapped structures and ~0.1 Å between the superimposed nutrient-loaded binding site shown in Figure 4B.

The sole major difference between the ligand-free and ligand-bound structures of LIVBP is clearly portrayed when one identical domain of the two different free structures and one bound structure is overlapped (Figure 3A). In both ligand-free structures, the two domains are well separated, and the cleft between the two domains is wide open and accessible to solvent. In sharp contrast, in the ligand-bound structure the lips of the two domains are in contact and, consequently, completely engulf the ligand in the cleft. The two ligand-free structures, distinguished as "open" and "superopen" forms, are related to the closed structures by a rigid body rotation between the two domains of about 50° and 60°, respectively, in the direction of the hinge-bending motion (discussed further below).

Table 4 and Figure 3B indicate the changes in the backbone torsion angles of the three interdomain connecting segments or hinges that accompany domain closure. The two major torsion angle changes (which are in the same direction and thus do not cancel) are confined to the ϕ_i and ψ_i of mainly two residues, Asp 123 in the first hinge and Phe 329 in the third hinge. For Asp 123, the averages of the ϕ/ψ changes (standard deviation in parentheses) are 41(5)°/32(3)° in going from the superopen to the three ligand-bound structures and 55(5)°/20(3)° in going from the open to the three ligand-bound structures. For Phe 329, the averages of the ϕ/ψ changes are 15(3)°/37(2)° and 12(3)°/34(2)° for the domain closures commencing from the superopen and open states, respectively. Despite the large backbone conformational differences of the two residues, their ϕ and ψ values in the two different open and three closed structures are in the normally allowed (minimum energy) region of the Ramachandran plots. The combined changes in the ϕ and ψ torsion angles of Asp 123 make larger contribution in the hinge bending than those of Phe 329 (Figure 3B). Whereas the change in ϕ is the major contributor of Asp 123, it is ψ for Phe 329 (Table 4). Thus, ϕ(123) and ψ(329) are the most important torsion angles in the hinge-bending motion, followed by ψ(123).

Although no single residue in segment 2 undergoes as large a change as the two described above in segments 1 and 3, the combined negative changes of about −25° of the ϕ and ψ of residue 250 (Figure 3B and Table 4) make appreciable contribution in going from the open to the ligand-bound state. The contribution is less in the domain closure commencing from the superopen state. There are several other relatively similar minor main chain torsion angle changes, especially in hinges 1 and 3 (Figure 3B), that contribute the remainder of the motion. One of these (residue 328) is observed in the hinge bending starting from the superopen state but not that commencing from the open state. Normal-mode analysis provides additional insight into the contributions of three hinges during domain closure and is discussed further below.

Aliphatic Amino Acid Binding. Each of the three bound amino acids exhibits well-defined difference electron density (Figure 4A). With the exception of one residue (Phe 276), which shows a small conformational change between the Leu- and Ile- or Val-bound structures, the configurations of the ligand-binding site in the three structures are extremely similar (Figure 4B). Moreover, the primary groups (α-ammonium and α-carboxylate, assuming normal p*K*s, and α-carbon) of the amino acids bound in the three structures superimpose very well. The same is true for the side chain

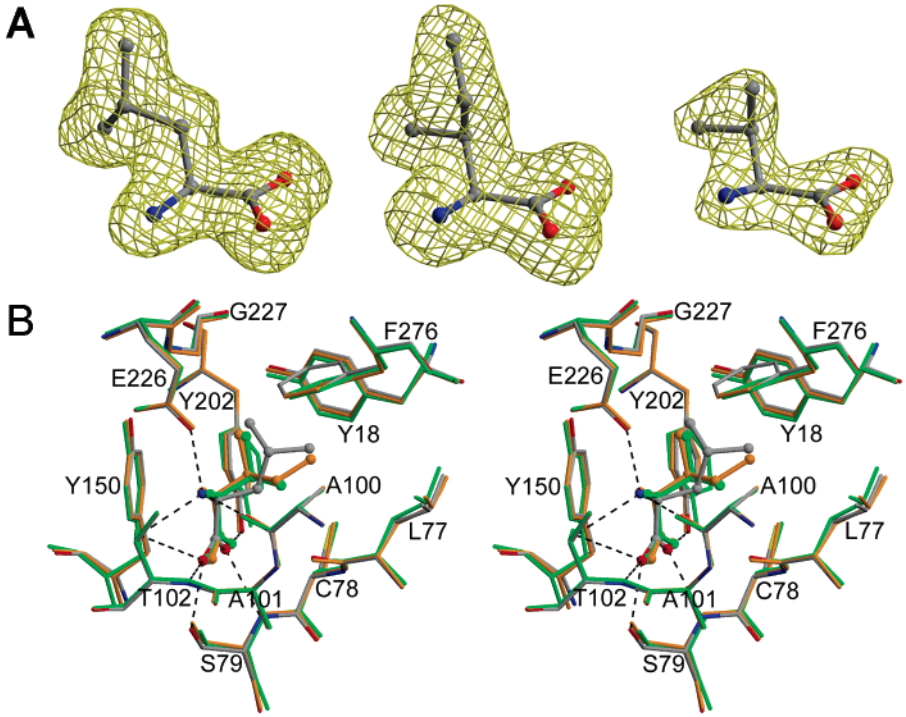

FIGURE 4: Binding of L-leucine, L-isoleucine, and L-valine to LIVBP. (A) $F_o - F_c$ omit maps for the bound Leu (left), Ile (middle), and Val (right) contoured at the 3σ level. (B) Superimposition of the binding site of the three structures (Table 1) with bound Leu (with color-coded atoms: oxygen, red; nitrogen, blue; and carbon, gray), Ile (yellow), and Val (green). Dashed lines represent hydrogen bonds.

Table 2: Hydrogen Bonds between LIVBP and L-Leucine, L-Isoleucine, or L-Valine

LIVBP			distance (<3.2 Å)		
atom	domain location	atom	Leu	Ile	Val
Ala 100 O	I	N	2.87	2.87	2.80
Thr 102 OG1	I	N	2.95	3.00	3.11
Glu 226 OE1[a]	II	N	2.68	2.71	2.64
Tyr 202 OH	II	OT1	2.77	2.63	2.66
Ser 79 N	I	OT1	2.87	2.90	2.94
Ser 79 OG	I	OT2	2.64	2.51	2.72
Thr 102 N	I	OT2	2.91	3.05	3.04
Thr 102 OG1	I	OT2	3.10	3.43[b]	3.48[b]

[a] The interaction of Glu 226 and the ammonium group of the amino acids is also a salt link. [b] Values exceed the distance limit.

Table 3: van der Waals Contacts between LIVBP and Amino Acids

LIVBP		no. of contacts (<4.5 Å) total/side chain only[a]		
residue	domain	Leu	Ile	Val
Tyr 18	I	14/14	12/12	5/5
Leu 77	I	10/6	9/6	9/5
Cys 78	I	7/1	12/3	9/2
Ser 79	I	10/0	10/0	10/0
Ala 100	I	9/4	11/7	10/5
Ala 101	I	6/0	5/0	7/1
Thr 102	I	8/0	8/0	8/0
Tyr 150	II	26/1	29/3	26/2
Tyr 202	II	11/4	12/6	11/5
Glu 226	II	7/4	7/4	7/4
Phe 276	I	8/8	7/7	4/4
total contacts		116/42	122/48	106/33

[a] Excluding the Cα carbon.

atoms (Cβ, Cγ1, and Cγ2) common to Ile and Val. Of the side chain atoms of Leu, only the Cδ1 and Cδ2 are close to the positions of Cδ1 and Cγ2 of Ile, respectively. The ligand-loaded binding site is completely devoid of water molecules (Figure 4B).

The amino acids are held in place by hydrogen bonds (Figure 4B and Table 2) and van der Waals interactions (Table 3). There are a total of eight hydrogen bonds, three with the α-ammonium group, one of which is also a salt link with Glu 226, and five with the α-carboxylate group. Similar polar interactions have been observed in the crystal structures of the complexes of leucine-specific binding protein with Leu (*33*).

The total number of van der Waals contacts made with the bound amino acids Leu and Ile varies slightly (116 and 122, respectively), but they clearly exceed that with Val (106). A similar pattern is also observed for the total contacts with only the side chains: almost the same numbers (42 and 48) for Leu and Ile, respectively, and considerably less (33) for Val. The side chains of the three aliphatic amino acid ligands are accommodated in a pocket formed by hydrophobic residues, mainly Tyr 18, Leu 77, Ala 100, and Phe 276 from domain I and Tyr 202 from domain II (Figure 4B and Table 3). The contacts made by these nonpolar residues contribute the most (>80%) to the total contacts with only the side chains. Once again, the nonpolar contacts with the side chains of Leu and Ile, which are nearly the same (36 and 38, respectively), are more abundant than those (28) with the Val side chain.

Judging by the data in Tables 2 and 3, domain I is dominant in binding the amino acids. It engages in six of the eight hydrogen bonds and in greater proportion of the total van der Waals contacts with Leu (72 of 116), Ile (74 of 122), and Val (62 of 106). Moreover, of the total contacts involving the five hydrophobic residues surrounding the side chains of the amino acids, almost all are made by those in domain I (32 of 36 with Leu, 32 of 38 with Ile, and 19 of

Table 4: Changes in Torsion Angles of the Three Connecting Segments Associated with Domain Closure[a]

segment/ residue		torsion angle change: superopen to ligand bound Leu	Ile	Val	open to ligand bound Leu	Ile	Val
segment 1							
Thr 118	ϕ	18	12	23	11	5	16
	ψ	−34	−32	−35	−30	−29	−31
Gly 119	ϕ	9	9	15	16	17	23
	ψ	−30	−29	−34	−28	−27	−28
Leu 120	ϕ	7	6	5	−5	−6	−7
	ψ	11	12	7	13	14	9
Asp 121	ϕ	23	22	23	21	20	21
	ψ	−34	−32	−35	−35	−33	−36
Ser 122	ϕ	23	22	21	29	28	26
	ψ	−16	−19	−8	−31	−34	−23
Asp 123	ϕ	**41**	**47**	**36**	**55**	**59**	**50**
	ψ	**34**	**32**	**29**	**23**	**20**	**17**
Gln 124	ϕ	−15	−9	−11	−17	−12	−13
	ψ	16	13	15	21	19	21
segment 2							
Pro 249	ϕ	18	19	11	13	14	6
	ψ	−25	−19	−19	−19	−13	−13
Lys 250	ϕ	−9	−17	−12	−12	−20	−15
	ψ	−10	2	−5	−19	−8	−14
Asn 251	ϕ	−12	−17	−17	3	−1	−2
	ψ	4	3	14	4	3	14
segment 3							
Gly 326	ϕ	4	4	2	−21	−22	−23
	ψ	−8	2	−6	2	13	4
Phe 327	ϕ	14	1	5	15	3	6
	ψ	−7	−9	−7	−1	−3	−2
Glu 328	ϕ	17	21	22	−3	0	1
	ψ	−2	−2	−7	2	1	−4
Phe 329	ϕ	**14**	**12**	**18**	**12**	**9**	**16**
	ψ	**39**	**37**	**35**	**36**	**34**	**32**
Gly 330	ϕ	11	7	7	3	−2	−2
	ψ	−11	−5	−4	−14	−8	−6

[a] Those in bold represent major changes.

24 with Val). Molecular dynamics simulations confirm the dominance of domain I in ligand binding (discussed further below).

Normal-Mode Analysis of Domain Closure and Targeted Molecular Dynamics (TMD) Simulations of Ligand Binding. To investigate the intrinsic flexibility of the protein structure that is likely to contribute to the observed large conformational change, we performed normal-mode analysis (*34*−*36*) on the open state of LIVBP. The result revealed two lowest frequency modes that are most relevant to the biological functions of LIVBP. Both modes describe motions around flexible hinge regions by rigid-body domain movements. The first lowest frequency mode (mode 7), shown in Figure 5A, is a classic hinge-bending mode (*35*). Starting from the open state (blue), if one bends the structure along this mode (following the arrow) toward the closed state, a conformation (green) that qualitatively resembles the closed state as shown in green in Figure 3A can be reached. The pattern of motion in this mode also reveals that the hinge of conformational changes in the protein is not located at a single point but is formed instead by a continuous region of amino acids primarily clustered around the three interdomain connecting segments. The second lowest frequency mode (mode 8) is a twisting mode around the hinge region. We observed that such a mode can be employed to describe the conformational change from the open state to the superopen state, in which a relative twist between the two domains is involved, in addition to the slight bending associated with the further opening of the hinge.

Further evidence for the dominance of domain I in ligand binding comes from TMD simulations. In the TMD simulations, the beginning and ending points are known, while the trajectory taken between them is simulated. In this case, the Ile-bound state of LIVBP served as the starting point and the open state served as the ending point, while the process of ligand unbinding was simulated. Ligand unbinding is essentially the reverse of ligand binding except the former involves multiple outcomes from a single starting point, while the latter involves a single outcome from multiple starting points and is thus more challenging to study in this instance. In all four of the simulations performed (each starting with a different random seed), the ligand remained bound to domain I during the opening of the cleft. Often the ligand was seen to retain some of the hydrogen bonds with the residues in domain I as observed in the bound complex crystal structures, although at increased distances reflecting the process of ligand unbinding, while others are replaced with hydrogen bonds to water. Figure 5B shows a stereo close-up view of one such instance where, as the cleft opens and the ligand is in the process of being released, only two of the original six hydrogen bonds between the bound Ile and domain I (Figure 3B and Table 2) are retained at or below 3.2 Å distances, although two more are found between 3.2 and 3.5 Å, and one new hydrogen bond to water is formed at Ile OT2, replacing the one to Thr 102 N. Moreover, the hydrogen bonds between Thr 102 N and Ile OT2 and Thr 102 OG1 and Ile N are lost. As expected, the two hydrogen bonds, including the salt link, involving domain II (Glu 226 OE1−Ile N and Tyr 202 OH−Ile OT1) are the first to be lost.

DISCUSSION

Open and Closed States of LIVBP. Since all three ligand-bound complexes crystallized in different space groups (Table 1), the very close similarity of their structures is independent of lattice forces. A previous small-angle X-ray scattering study of LIVBP in the presence and absence of bound ligands has indicated the existence of both open and closed states in solution (*37*). These results, combined with the two ligand-free structures, are unequivocal evidence that the open and closed states exist in equilibrium in physiological conditions. The presence of ligand drives the equilibrium predominantly toward the closed state.

The two different open state structures, together with the very similar ligand-bound structures, indicate the trajectory or pathway that the motion takes from the open to the closed states of the protein. On the basis of the data shown in Table 4 and Figure 3, especially highlighting the two major changes in the torsion angles, hinge 1 undergoes the greatest change, followed by hinge 3. Hinge 2, which is also the shortest, experiences the least alteration.

From a structural standpoint, the bending motion of a hinge between the two domains is now a firmly established feature of the ABC-transport binding protein family. Multiple open structures of the ribose- and allose-binding proteins have also been observed (*38*, *39*). Besides these two monosaccharide-binding proteins and LIVBP, crystal structures of the closed and open states of several other ABC-transport binding

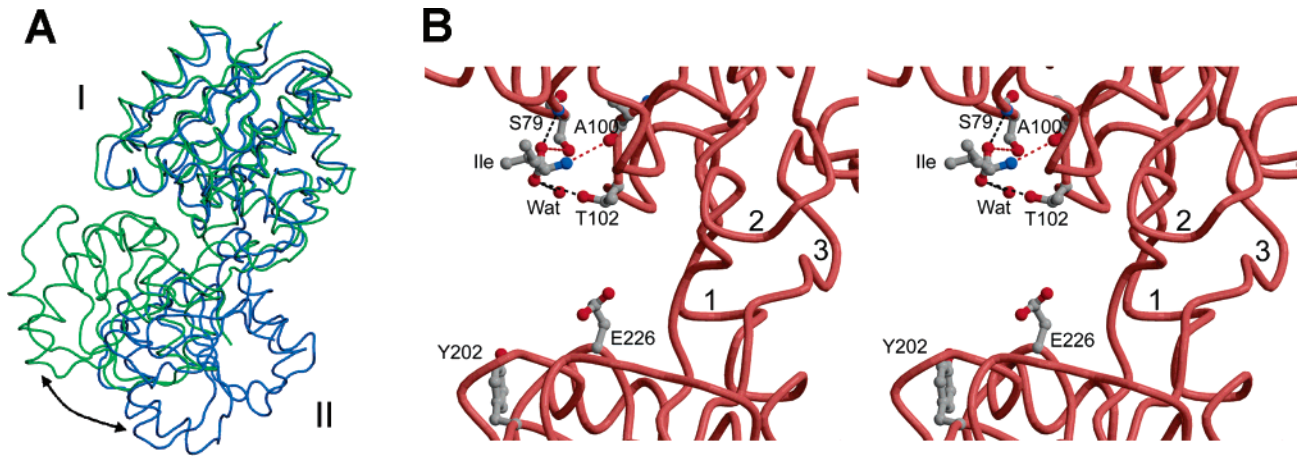

FIGURE 5: Normal-mode analysis of domain closure and targeted molecular dynamics (TMD) simulation of ligand binding. (A) Normal-mode analysis. The analysis reveals that the lowest frequency, hinge-bending mode captures the structural differences between the open and closed states of LIVBP. If the open state (blue) is bent along this mode (arrow), a conformation (green) is reached that qualitatively resembles the closed state (green in Figure 3A). The superimposition of domain I shown here is poor due to the fact that the pseudoclosed conformation (green) is neither a crystal structure nor an energy-minimized conformation but is merely a "bent" version of the open state. The orientation is similar to that shown in Figure 3A. (B) Stereo close-up view of the ligand-binding cleft between the two domains (I, top, and II, bottom) at a snapshot taken during one of the TMD simulations. This view shows that the two domains have already separated but the isoleucine remains bound to domain I, albeit more loosely than in the closed state. In all four simulations performed the ligand remained bound to domain I rather than domain II. This example demonstrates the loss of some of the hydrogen bonds seen between the ligand and the closed state of LIVBP (Figure 4 and Table 2) and the replacement of others by the formation of hydrogen bonds to water. Hydrogen bonds are shown in dotted lines (red, <3.2 Å distances, and black, 3.2−3.5 Å). Wat represents a water molecule. The three hinges are identified with numbers 1, 2, and 3.

proteins have also been determined, including those with specificities for maltooligosaccharides (maltose to maltoheptaose) (*40*, *41*), lysine/arginine/ornithine (*42*), leucine (*33*), dipeptides (*43*), oligopepetide (*44*), phosphate (*45*, *46*), glutamine (*47*, *48*), and nickel (*49*). The bending angles that relate the closed and open states vary, 60° and 50° for LIVBP (38 kDa), 55−50° for the dipeptide-binding protein (57 kDa), Lys/Arg/Orn-binding protein (26 kDa), and Gln-binding protein (25 kDa), 55° and 40° for the leucine-specific binding protein, 45° for the allose- and ribose-binding proteins (30 kDa), 35° for the maltose-binding protein (41 kDa), 25° for the phosphate-binding protein (35 kDa) and the oligopeptide-binding protein (57 kDa), and 15° for the nickel-binding protein (56 kDa). It is apparent that there are no correlations between the magnitudes (from the largest to the smallest) of the bending angles and the protein masses or the ligand sizes, except for the smallest (nickel). The differences in the bending angles could reflect crystal lattice effects which would affect the open forms the most. Interestingly, there is no correlation between the bending angles and the number of crossover segments between the two domains, three crossovers for LIVBP and maltose-, galactose-, allose-, ribose-, and phosphate-binding proteins and two crossovers for the dipeptide-, oligopeptide-, Lys/Arg/Orn-, Gln-, and nickel-binding proteins. Even the top half (60−45°) and bottom half (35−15°) of the bending angles cannot be correlated with the number of crossovers. These observations indicate that the number of crossovers, at least up to three based on data reported here, does not place much constraint on the interdomain rotation.

LIVBP provides a clear example that multidomain proteins have evolved in such a way that the pathways of functionally important conformational changes follow the low-frequency normal modes of the structures (*50*). This is because it costs the least amount of energy to fulfill the conformational changes along the intrinsic modes. This can be seen from the fact that, as demonstrated in Figure 5A, the extent of conformational change (amplitude) that can be described by a single low-frequency normal mode is much larger than that of equilibrium thermal fluctuation of an harmonic oscillator at 300 K (*50*). During the binding process, the favorable energetic interactions between the ligand and protein substantially and continuously lower the energy barrier along the conformational changes so as to make such a large pseudoharmonic conformational deformation possible. This mechanistic picture regarding the energy landscape along the conformational pathway is likely to be applicable to many large protein complexes such as motor proteins in which ligand-induced large domain movements play an important role in their functions.

Hinge bending between domains of proteins is an important factor in the functions of a wide variety of proteins. This motion for many bilobate proteins and domains is associated solely with ligand/substrate binding, which in enzymes further initiates catalysis. In addition to ligand binding, interdomain rotation in the superfamily of binding proteins of the ABC-transport systems also fulfills a key role in signal transduction by forming a unique ligand-stabilized closed state structure which is then recognized preferentially by the cytoplasmic membrane-bound components and thereby triggers active transport or, in the case of the binding protein-dependent chemotaxis, changes in flagellar rotational direction (*5*, *40*). The two domains of the binding proteins are apparently involved in the interactions with the active transport and chemotaxis membrane components (*40*, *51*), which serve as sensors for productive binding with the membrane components.

Ligand Binding: Polar versus Nonpolar Interactions. One other important outcome of the determination of the crystal structures reported here is the atomic details of the binding of the three aliphatic amino acids. Due to the juxtapositioning of functional polar groups that interact via the highly

directional hydrogen bonds with the primary ammonium and carboxylate groups of the amino acids and the presence of the hydrophobic pocket that harbors the amino acid side chain, the binding site, fully formed following cleft closure, is tailored made for only amino acids in the L configuration. This finding is consistent with previous results indicating that LIVBP does not bind aliphatic amino acids with modified primary groups (e.g., L-α-aminobutyrate, L-norvaline, and L-alloisoleucine) (*52*). The nonpolar nature of the pocket in the binding site for harboring the side chain of the bound amino acids is completely in accord with the specificity of the protein for the branched chain aliphatic amino acids.

The observation that more polar interactions are associated with the α-carboxylate (five versus three with the α-ammonium) of the amino acids is intriguing since they are made entirely with main chain NH and side chain OH hydrogen bond donor groups (Figure 4B and Table 2). This is reminiscent of the original discovery of the involvement of the same types of protein donor or dipolar groups in the interaction between the completely buried and desolvated sulfate dianion and its receptor of the ABC-type sulfate transporter (*53*). Obviously, this type of interaction between an ion and polar groups with only partial charges [which we have called "ion−dipole interaction" (*54*, *55*)] is sufficient to overcome the hydration energy of ions (as much as −260 kcal mol^{-1} experimentally determined for sulfate) and to compensate for the charge of the completely buried and dehydrated ions. Since its discovery almost 20 years ago, ion−dipole interaction has been observed in a variety of contexts in proteins, including structures, enzyme catalysis, ion transport, and channeling (for examples, see ref *55*). A notable feature fairly common to this interaction is the simultaneous involvement of Ser or Thr side chain OH groups as a donor or acceptor or both and its main chain NH (e.g., Thr 102 and Ser 79 as shown in Figure 4B and Table 2) or associated peptide bond carbonyl oxygen (for many more examples, see ref *55*).

As expected, the Val side chain makes fewer van der Waals contacts with the protein than those of Ile and Leu (Table 3). Differences in the number of contacts with the ligands (Table 3) could account for the differences, albeit small, in the dissociation constants for the binding of Leu (2.3 μM), Ile (0.9 μM), and Val (4 μM) determined for purified LIVBP, which has been verified to be free of bound endogenous ligand (see also ref *15*).

The clear dominance of domain I in ligand binding, by way of both polar and nonpolar interactions (Tables 2 and 3), indicates that this domain is the initial site of ligand binding in the open state and, thus, governs ligand specificity. This is also consistent with the finding of leucine binding to the same domain exclusively in the structure of an LIVBP crystal of the open state soaked in a solution containing leucine (*8*) and with the observed binding of isoleucine to this domain in the targeted molecular dyanamics simulations described above. Interestingly, whereas domain I provides six of the seven polar groups with no formal charges that make hydrogen bonds with the ligands, domain II deploys the negatively charged residue (Glu 226) that makes a salt link with the α-ammonium group, as well as the other hydrogen-bonding group (OH of Tyr 202) (Table 2). The collection of several polar groups with only partial charges in domain I is apparently more effective in attracting the zwitterionic ligands than the combination of the carboxylate of Glu 226 and hydroxyl of Tyr 202 in domain II. It is also apparently more effective in holding onto the ligand momentarily as the two domains open in the targeted molecular dynamics simulations.

LIVBP is second only to the maltose- (or maltooligosaccharide-) binding protein (MalE) (*40*, *41*, *56*) of the superfamily of the ABC-transporter binding proteins for which the crystal structures of all possible functionally important conformations have been determined: the open ligand-free, open ligand-bound, and the closed ligand-bound states. These structures give credence to the ligand-binding kinetic studies in solution demonstrating a two-step mechanism: ligand first binds very rapidly (on rates close to diffusion rate limit) in the open state and then the bound open state intermediate isomerizes to the closed state (*57*). For the phosphate-binding protein, the rate of the domain closure is about 290 s^{-1} (*57*).

Although the aliphatic amino acids and maltooligosaccharides are different sets of amphipathic nutrients, they share a common feature by binding preferentially to the domain whose site is more nonpolar in character than that of the other domain. In fact, the site of the domain in maltose-binding protein for initial binding is overwhelmingly hydrophobic since it provides all of the aromatic residues that stack against nonpolar patches from clusters of sugar ring CH bonds and only one hydrogen-bonding polar group (*56*). Apparently, although the oligosaccharides are highly polar, containing about two to three times more accessible polar surface (from exocylic OH groups) than nonpolar surface patches, initial binding does not favor the other domain which provides almost all of the many charged and neutral polar groups that make the majority of hydrogen bonds with the sugar hydroxyl groups and thus might have been expected to govern ligand specificity. In the match between the two very different domains, the one with the nonpolar site apparently prevails over the other with the polar site. This seems at variance with the popular view that polar groups operate over long range, initially providing the driving force to attract the ligand, whereas nonpolar groups operate over short range, taking over when the protein and ligand come into sufficient close proximity. This mechanism could be applicable to LIVBP since domain I engages in a much larger number of both ion−dipole (no salt link) and nonpolar interactions with the zwitterionic aliphatic amino acids. Nevertheless, nonpolar interactions with domain I clearly outnumber polar interactions (Tables 2 and 3). Of the other nutrients, the tetrahedral oxyanions such as sulfate and phosphate represent the extreme case since they are bound by polar interactions in their respective binding proteins and have as solutes very much greater hydration energies.

Paradoxically, although the ligands (aliphatic amino acid zwitterions, neutral carbohydrates, and oxyanions) and their modes of binding are entirely different, they are bound with similar affinities (K_a values in the low micromolecular range). In fact, the same holds true for the other diverse ligands of all but a few of the other members of this protein superfamily. The major factor that confers this feature, which is likely crucial to the role of the protein superfamily in active transport and chemotaxis (*58*−*59*), remains to be explored. Could it be domain closure?

REFERENCES

1. Kanehisa, M., Goto, S., Kawashima, S., Okuno, Y., and Hattori, M. (2004) The KEGG resource for deciphering the genome, *Nucleic Acids Res. 32* (Database issue), D277−D280.
2. Saier, M. H., Jr. (2000) A functional-phylogenetic classification system for transmembrane solute transporters, *Microbiol. Mol. Biol. Rev. 64*, 354−411.
3. Nikaido, H. (1994) Maltose transport system of *Escherichia coli*: an ABC-type transporter, *FEBS Lett. 246*, 55−58.
4. Payne, J. W., and Smith, M. W. (1994) Peptide transport by microorganisms, *Adv. Microb. Physiol. 36*, 1−80.
5. Quiocho, F. A., and Ledvina, P. S. (1996) Atomic structure and specificity of bacterial periplasmic receptors for active transport and chemotaxis: variation of common themes, *Mol. Microbiol. 20*, 17−25.
6. Adams, M. D., Wagner, L. M., Graddis, T. J., Landick, R., Antonucci, T. K., Gibson, A. L., and Oxender, D. L. (1990) Nucleotide sequence and genetic characterization reveal six essential genes for the LIV-I and LS transport systems of *Escherichia coli*, *J. Biol. Chem. 265*, 11436−11443.
7. Sack, J. S., Trakhanov, S. D., Tsigannik, I. H., and Quiocho, F. A. (1989) Structure of the L-leucine-binding protein refined at 2.4 Å resolution and comparison with the Leu/Ile/Val-binding protein structure, *J. Mol. Biol. 206*, 193−207.
8. Sack, J. S., Saper, M. A., and Quiocho, F. A. (1989) Periplasmic binding protein structure and function. Refined X-ray structures of the leucine/isoleucine/valine-binding protein and its complex with leucine, *J. Mol. Biol. 206*, 171−191.
9. Gilliland, G. L., and Quiocho, F. A. (1981) Structure of the L-arabinose-binding protein from *Escherichia coli* at 2.4 Å resolution, *J. Mol. Biol. 146*, 341−362.
10. Quiocho, F. A., and Vyas, N. K. (1984) Novel stereospecificity of the L-arabinose-binding protein, *Nature 310*, 381−386.
11. Vyas, N. K., Vyas, M. N., and Quiocho, F. A. (1983) The 3 Å resolution structure of a D-galactose-binding protein for transport and chemotaxis in *Escherichia coli*, *Proc. Natl. Acad. Sci. U.S.A. 80*, 1792−1796.
12. Vyas, N. K., Vyas, M. N., and Quiocho, F. A. (1988) Sugar and signal-transducer binding sites of the *Escherichia coli* galactose chemoreceptor protein, *Science 242*, 1290−1295.
13. Mao, B., Pear, M. R., McCammon, J. A., and Quiocho, F. A. (1982) Hinge-bending in L-arabinose-binding protein: The "Venus's-flytrap" model, *J. Biol. Chem. 257*, 1131−1133.
14. Trakhanov, S., and Quiocho, F. A. (1995) Influence of divalent cations in protein crystallization, *Protein Sci. 4*, 1914−1919.
15. Vorotyntseva, T. I., Surin, A. M., Trakhanov, S. D., Nabiev, I. R., and Antonov, V. K. (1981) Spectral properties of the leucine-isoleucine-valine binding protein and its complexes with substrates, *Bioorg. Khim. 7*, 45−57.
16. Fitzgerald, P. M. D. (1988) MERLOT Manual, Merck Sharp & Dhome Laboratories, Rahway, NJ.
17. Brünger, A. T. (1992) *X-PLOR, Version 3.1, A system for X-ray crystallography and NMR*, Yale University, New Haven, CT.
18. Brünger, A. T., Adams, P. D., Clore, G. M., DeLano, W. L., Gros, P., Grosse-Kunstleve, R. W., Jiang, J. S., Kuszewski, J., Nilges, M., Pannu, N. S., Read, R. J., Rice, L. M., Simonson, T., and Warren, G. L. (1998) Crystallography & NMR system: A new software suite for macromolecular structure determination, *Acta Crystallogr. D 54*, 905−921.
19. Sack, J. S., and Quiocho, F. A. (1997) CHAIN-A crystallographic modeling program, *Methods Enzymol. 277*, 158−173.
20. Yao, N., Trakhanov, S., and Quiocho, F. A. (1994) Refined 1.89-Å structure of the histidine-binding protein complexed with histidine and its relationship with many other active transport/chemosensory proteins, *Biochemistry 33*, 4769−4779.
21. Lamzin, V. S., and Wilson, K. S. (1997) Automated refinement for protein crystallography, *Methods Enzymol. 277*, 269−305.
22. Brooks, B. R., Bruccoleri, R. E., Olafson, B. D., States, D. J., Swaminathan, S., and Karplus, M. (1983) CHARMM: A program for macromolecular energy, minimization, and dynamics calculations, *J. Comput. Chem. 4*, 187−217.
23. Neria, E., Fischer, S., and Karplus, M. (1996) Simulation of activation free energies in molecular systems, *J. Chem. Phys. 105*, 1902−1921.
24. Schlitter, J., Engels, M., Kruger, P., Jacoby, E. U., and Wollmer, A. (1993) Targeted molecular dynamics simulation of conformational change: application to the T−R transition in insulin, *Mol. Simul. 10*, 291−308.
25. Jorgensen, W. L. (1981) Transferable intermolecular potential functions for water, alcohols, and ethers. Application to liquid water, *J. Am. Chem. Soc. 103*, 335−340.
26. Ryckaert, J. P., Ciccotti, G., and Berendsen, H. J. C. (1977) Numerical integration of the Cartesian equations of motion of a system with constraints: molecular dynamics of *n*-alkanes, *J. Comput. Phys. 23*, 327−341.
27. Kraulis, P. J. (1991) MOLSCRIPT: A program to produce both detailed and schematic plots of protein structures, *J. Appl. Crystallogr. 24*, 946−950.
28. Humphrey, W., Dalke, A., and Schulten, K. (1996) VMD−Visual molecular dynamics, *J. Mol. Graphics 14*, 33−38.
29. Ovchinnikov, Y. A., Aldanova, N. A., Arzamazova, N. M., and Moroz, I. N. (1977) The primary structure of Leu, Ile and Val (LIV)-binding protein from *Escherichia coli*, *FEBS Lett. 78*, 313−316.
30. Landick, R., and Oxender, D. L. (1985) The complete nucleotide sequences of the *Escherichia coli* LIV-BP and LS-BP genes. Implications for the mechanism of high-affinity branched-chain amino acid transport, *J. Biol. Chem. 260*, 8257−8261.
31. Steward, D. E., Sarkar, A., and Wampler, J. E. (1990) Occurrence and role of cis peptide bonds in protein structures, *J. Mol. Biol. 214*, 253−260.
32. Pal, D., and Chakrabarti, P. (1999) Cis peptide bonds in proteins: Residues involved, their conformations, interactions and locations, *J. Mol. Biol. 294*, 271−288.
33. Magnusson, U., Salopek-Sondi, B., Luck, L. A., and Mowbray, S. L. (2004) X-ray structures of the leucine-binding protein illustrate conformational changes and the basis of ligand specificity, *J. Biol. Chem. 279*, 8747−8752.
34. Brooks, B. R., Janez¢ic, D., and Karplus, M. (1995) Harmonic analysis of large systems. I. Methodology, *J. Comput. Chem. 16*, 1522−1542.
35. Brooks, B., and Karplus, M. (1985) Normal modes for specific motions of macromolecules: Application to the hinge-bending mode of lysozyme, *Proc. Natl. Acad. Sci. U.S.A. 82*, 4995−4999.
36. Levitt, M., Sander, C., and Stern, P. S. (1985) Protein normal-mode dynamics: Trypsin inhibitor, crambin, ribonuclease and lysozyme, *J. Mol. Biol. 181*, 423−447.
37. Olah, G. A., Trakhanov, S., Trewhella, J., and Quiocho, F. A. (1993) Leucine/isoleucine/valine-binding protein contracts upon binding of ligand, *J. Biol. Chem. 268*, 16241−16247.
38. Bjorkman, A. J., and Mowbray, S. L. (1998) Multiple open forms of ribose-binding protein trace the path of its conformational change, *J. Mol. Biol. 279*, 651−664.
39. Magnusson, U., Chaudhuri, B. N., Ko, J., Park, C., Jones, T. A., and Mowbray, S. L. (2002) Hinge-bending motion of D-allose-binding protein from *Escherichia coli*, *J. Biol. Chem. 277*, 14077−14084.
40. Spurlino, J. C., Lu, G. Y., and Quiocho, F. A. (1991) The 2.3-Å resolution structure of the maltose- or maltodextrin-binding protein, a primary receptor of bacterial active transport and chemotaxis, *J. Biol. Chem. 266*, 5202−5219.
41. Sharff, A. J., Rodseth, L. E., Spurlino, J. C., and Quiocho, F. A. (1992) Crystallographic evidence of a large ligand-induced hinge-twist motion between the two domains of the maltodextrin binding protein involved in active transport and chemotaxis, *Biochemistry 31*, 10657−10663.
42. Oh, B. H., Pandit, J., Kang, C. H., Nikaido, K., Gokcen, S., Ames, G. F.-L., and Kim, S. H. (1993) Three-dimensional structures of the periplasmic lysine/arginine/ornithine-binding protein with and without a ligand, *J. Biol. Chem. 268*, 11348−11355.
43. Nickitenko, A. V., Trakhanov, S., and Quiocho, F. A. (1995) 2 Å resolution structure of DppA, a periplasmic dipeptide transport/chemosensory receptor, *Biochemistry 34*, 16585−16595.
44. Sleigh, S. H., Tame, J. R., Dodson, E. J., and Wilkinson, A. J. (1997) Peptide binding in OppA, the crystal structures of the periplasmic oligopeptide binding protein in the unliganded form and in complex with lysyllysine, *Biochemistry 36*, 9747−9758.
45. Luecke, H., and Quiocho, F. A. (1990) High specificity of a phosphate transport protein determined by hydrogen bonds, *Nature 347*, 402−406.
46. Ledvina, P. S., Yao, N., Choudhary, A., and Quiocho, F. A. (1996) Negative electrostatic surface potential of protein sites specific for anionic ligands, *Proc. Natl. Acad. Sci. U.S.A 93*, 6786−6791.

47. Sun, Y.-J., Rose, J., Wang, B.-C., and Hsiao, C.-D. (1998) The structure of glutamine-binding protein complexed with glutamine at 1.94 Å resolution: comparisons with other amino acid binding proteins, *J. Mol. Biol. 278*, 219−229.
48. Hsiao, C. D., Sun, Y. J., Rose, J., and Wang, B. C. (1996) The crystal structure of the glutamine-binding protein from *Escherichia coli*, *J. Mol. Biol. 262*, 225−242.
49. Heddle, J., Scott, D. J., Unzai, S., Park, S. Y., and Tame, J. R. (2003) Crystal structures of the liganded and unliganded nickel-binding protein NikA from *Escherichia coli*, *J. Biol. Chem. 278*, 50322−50329.
50. Ma, J. (2004) New advances in normal mode analysis of supermolecular complexes and applications to structural refinement, *Curr. Protein Pept. Sci. 5*, 119−123.
51. Martineau, P., Saurin, W., Hofnung, M., Spurlino, J. C., and Quiocho, F. A. (1990) Progress in the identification of interaction sites on the periplasmic maltose binding protein from *E. coli*, *Biochimie 72*, 397−402.
52. Amanuma, H., and Anraku, Y. (1974) Transport of sugars and amino acids in bacteria. XII. Substrate specificities of the branched chain amino acid-binding proteins of *Escherichia coli*, *J. Biochem. (Tokyo) 76*, 1165−1173.
53. Pflugrath, J. W., and Quiocho, F. A. (1985) Sulphate sequestered in the sulfate-binding protein is bound solely by hydrogen bonds, *Nature 314*, 257−260.
54. He, J. J., and Quiocho, F. A. (1993) Dominant role of local dipoles in stabilizing uncompensated charges on a sulfate sequestered in a periplasmic active transport protein, *Protein Sci. 2*, 1643−1647.
55. Vyas, N. K., Vyas, M. N., and Quiocho, F. A. (2003) Crystal structure of *M. tuberculosis* ABC phosphate transport receptor: specificity and charge compensation dominated by ion−dipole interactions, *Structure 11*, 765−774.
56. Duan, X., and Quiocho, F. A. (2002) Structural evidence for the dominant role of nonpolar interactions in the binding of a transport/chemonsensory receptor to its highly polar ligands, *Biochemistry 41*, 706−712.
57. Ledvina, P. S., Tsai, A. L., Wang, Z., Koehl, E., and Quiocho, F. A. (1998) Dominant role of local dipolar interactions in phosphate binding to a receptor cleft with an electronegative charge surface: equilibrium, kinetic, and crystallographic studies, *Protein Sci. 7*, 2550−2559.
58. Miller, D. M., III, Olson, J. S., Pflugrath, J. W., and Quiocho, F. A. (1983) Rates of ligand binding to periplasmic proteins involved in bacterial transport and chemotaxis, *J. Biol. Chem. 258*, 13665−13672.
59. Quiocho, F. A. (1990) Atomic structures of periplasmic binding proteins and the high-affinity active transport system in bacteria, *Philos. Trans. R. Soc. London 326*, 341−351.

BI047302O